Energy 240 (2022) 122475

Contents lists available at ScienceDirect

Energy

journal homepage: www.elsevier.com/locate/energy

Study on pressurized isothermal pyrolysis characteristics of low-rank coal in a pressurized micro-fluidized bed reaction analyzer

Yao Zhu, Qinhui Wang*, Kaikun Li, Jianmeng Cen, Mengxiang Fang, Chengdong Ying

State Key Laboratory of Clean Energy Utilization, Zhejiang University, Hangzhou, 310027, China

ARTICLE INFO

Article history:
Received 30 June 2021
Received in revised form
6 October 2021
Accepted 28 October 2021
Available online 29 October 2021

Keywords:
Pressurized pyrolysis
Isothermal kinetics
Pressurized micro-fluidized bed reaction analyzer
Gas-releasing characteristics

ABSTRACT

In order to investigate the pressurized isothermal pyrolysis characteristics of coal, the effect of pressure on gas release characteristics and the kinetics of pressurized isothermal pyrolysis are explored for the first time in a pressurized micro-fluidized bed reaction analyzer (P-MFBRA). This work finds that the yields of CO_2, CO, CH_4, and H_2 increases with temperature and pressure. The difference in the order of gas-releasing reduces as temperature and pressure rises, but that of gas-ending first decreases and then increases with pressure. The most probable mechanism functions of CO_2, CO and CH_4 change from shrinking core model to homogeneous model at 1 MPa, 0.8 MPa and 0.5 MPa, respectively, showing that reaction is controlled by chemistry under low pressure but affected by diffusion effect with elevating pressure. The rate constant and activation energy (Ea) of each gas appear an increasing-decreasing tendency and the difference between Ea of each gas reduces with pressure. Compared with non-isothermal experiments, the Ea (20.8–475 kJ mol^{-1}) and pre-exponential factor in P-MFBRA are less than those (70–150 kJ mol^{-1}) in the pressurized thermogravimetric analyzer (P-TGA), indicating P-MFBRA can effectively reduce the diffusion inhibition, and the kinetics obtained is close to the reaction in industrial fluidized bed reactor.

1. Introduction

Coal consumption accounted for 30% of the world's total energy consumption in 2013 [1]. China consumed 2.738 billion tons of coal (standard coal) in 2015, accounting for about 50% of the world's total coal consumption [2], and coal continue to occupy a considerable proportion in China energy distribution, with about 59% of energy consumption in 2018 [3]. However, traditional coal utilization methods emit a large amount of pollutants and CO_2, which seriously aggravates environmental pollution and the greenhouse effect [4]. Therefore, it is urgent to develop clean and efficient coal utilization technologies. In recent years, integrated gasification combined cycle technology (IGCC) and pressurized fluidized bed combustion (PFBC) have attracted widespread attention, among which PFBC is an effective way with CO_2 capture and storage [5]. Pressurized gasification and combustion are not only the key steps of these two technologies, but also a better way to improve the reaction rate and productivity [5,6]. Pyrolysis conditions have a great impact on the char yield and properties, thereby affecting the reactivity of char gasification and combustion [5,7]. Therefore, strengthening the understanding for the pressurized pyrolysis process and proper modeling are essential for the development and improvement of the design and operation of the pressurized coal conversion process. However, there is still a lack of relevant basic data for coal pressurized pyrolysis, especially for the pressurized pyrolysis of low-rank coal.

Reaction kinetic is a common method to analyze pyrolysis process, which can reveal the reaction mechanism and product characteristics, provide guidance for the design of industrial reactors, and optimize operating conditions [7,8]. The pyrolysis process is conducted simultaneously through a series of complex competitive reactions, so the exact mechanism remains controversial [9]. Hence, it is necessary to deeply understand heterogeneous gas-solid reaction to obtain reliable kinetic data.

Based on the reaction temperature, gas-solid reactions are divided into non-isothermal and isothermal reaction [10]. Non-isothermal reaction based on thermogravimetric analyzer (TGA) can ensure that there are no missing temperature zones [11]. Whereas, thermogravimetry (TG) cannot be operated at high gas velocity and high heating rate limited by its structure, causing

* Corresponding author.
E-mail address: qhwang@zju.edu.cn (Q. Wang).

https://doi.org/10.1016/j.energy.2021.122475
0360-5442/

serious diffusion limitations for reaction [12]. Meanwhile, the kinetics parameters of samples whose structure changes with temperature cannot be measured at a certain temperature [13,14]. Because pyrolysis reaction is very rapid, the reaction process is difficult to accurately determine the reaction time and the release sequence for gas products [14]. Therefore, relevant researchers use their own methods to obtain the required reaction kinetic parameters. Zabaniotou et al. has carried out fast pyrolysis experiment in a laboratory wire mesh reactor and found the pyrolysis rate can be simulated by a kinetic scheme involving two parallel reactions [15]. Manya et al. conducted isothermal pyrolysis experiments in an improved system and proposed a new kinetic method [16]. Those make the data is fragmented, unsystematic, and different [13,17]. The diffusion phenomenon is more severe under pressurized conditions that the actual calculation results are affected. Table 1 summarizes the relevant literatures on pressurized pyrolysis, and it can find that the existing studies for the kinetics of pressurized pyrolysis are conducted with P-TGA. The actual pressurized pyrolysis process is basically an instantaneous reaction. However, the reaction time under pressurization is longer than atmosphere in P-TGA, so the results of P-TGA are directly affected by the reaction time, making the relevant data deviate from the real reactions in industrial reactors. The research of pressurized isothermal pyrolysis is basically carried out in fixed bed, mainly studying the influence of pressure on yield and char physicochemical characteristics. There are few studies on the effect of pressure on the thermochemical behavior and gas evolution state of isothermal pyrolysis process, so the content of the pressurized isothermal pyrolysis kinetics must be supplemented.

The micro-fluidized bed reaction analyzer (MFBRA) can solve the above problems. The specific structure and principle of MFBRA are described in detail in the literature [14]. MFBRA adopts a micro fluidized bed as the reactor, pulse instantaneous feeding and fast mass spectrometry to detect the release characteristics of gas products online. It realizes a low-diffusion isothermal reaction and is suitable for experiments at any reaction temperature. The calculated kinetic parameters are closer to intrinsic values [30]. So far, MFBRA has been widely used [17,31], but there is almost no research on P-MFBRA. In this work, low-rank coal is used as the raw material, and the pressurized isothermal pyrolysis experiment is conducted in P-MFBRA for the first time, making the reaction closer to the actual state. The release characteristics of gas products at different temperatures and pressures are studied, different models are used to fit the experimental results, the isothermal pyrolysis kinetic parameters are calculated, and the reaction mechanism is analyzed, to supply the research content of low-rank coal pressurized isothermal kinetics. Finally, it is compared with the results of pressurized non-isothermal experiments reported in literatures to provide guidance for the design of pressurized reactors.

2. Materials and methods

2.1. Materials

Naomao Hu coal, a typical Xinjiang coal type, was took as the experimental sample and ground and sieved to a particle size range of 75–125 μm. The properties of the coal samples are shown in Table 2. The coal samples were dried at 105 °C for 24 h to remove the moisture before pyrolysis experiments.

2.2. Experimental equipment and methods

The schematic diagram of the P-MFBRA system is shown in Fig. 1, that mainly consists of pulse feeding system, pressurized micro fluidized bed reactor, gas supply unit, gas purification system, and software control system. The sample feeding system is driven by an electromagnetic valve, and the sample is injected into the reactor by pulsed gas in less than 0.1s. The pulse pressure is ~0.2 MPa under atmosphere but it needs to be determined in accordance with pyrolysis pressure at pressurized conditions. The micro fluidized bed reactor is made of high temperature and pressure resistant metal, whose inner diameter is 15 mm and length of reaction zone is 150 mm. The fluidized medium is silica sand with average diameter of 100–150 μm. The generated gas product quickly escapes from the reactor, after filtering, condensing, and drying, a small amount passes into the fast mass spectrometry (MS, AMETEK), and the remaining amount is measured by the dry flowmeter to determine the total volume. The gas is collected through a gas bag and detected by a micro gas chromatography (GC, Agilent 3000 A) to obtain the yields of the main gas components. Parameters such as fluidizing gas volume, pulse time, pyrolysis temperature, etc. are all controlled by software, and pressure is controlled by a backpressure valve and software.

Weigh 5.8 g of silica sand into the bottom of the reactor, connect all gas lines, purge the system and check the air tightness. After heating the reactor to preset pyrolysis temperature with a temperature fluctuation of less than ±5 °C, a certain amount of sample is put into the feed container, the backpressure valve is closed, pressure increases to the experimental pressure and then the backpressure valve is adjusted to keep pressure stable. Ar and N_2 are used for the pulse gas and experimental gas respectively. After pressure and temperature stabilization and the fluidization medium being in a uniform fluidization state, the sample is quickly injected into the reactor. The release characteristics of the main pyrolysis gases (CO_2, CO, CH_4 and H_2) are continuously measured with MS online. A gas bag is used to collect all the generated gases for analysis with GC. According to the measured data for MS and GC, the product composition, gas concentration and gas reaction

Table 1
Summary of literatures on pressurized pyrolysis.

Sample	Equipment	Conditions	Research content	Ref.
Bituminous coal	P-TGA	0.1–1.3 MPa	Kinetics of pressurized non-isothermal pyrolysis	[18]
Shenfu coal	P-TGA	0.1–5.0 MPa	Kinetics of pressurized non-isothermal pyrolysis	[19]
Lignite	P-TGA	0.1–4.0 MPa	Study on the kinetics of pressurized non-isothermal pyrolysis	[20]
Lignite	P-TGA	0.1–2.0 MPa	Thermogravimetric behavior during pyrolysis was studied	[21]
Coal	P-TGA	0.1–4.0 MPa	Study on the kinetics of pressurized non-isothermal pyrolysis	[22]
Low-rank coal	Pressurized fixed bed	0.1–0.5 MPa	Yield distribution of pyrolysis products	[23]
HLH coal	Pressurized fixed bed	0.1–1.0 MPa	Product distribution and char morphology	[24]
Bituminous coal	Pressurized entrained-flow reactor	0.1–4.0 MPa	Pressure on the carbon structure	[25]
Bituminous coal	Pressurized drop tube furnace	0.1–1.2 MPa	The effects of pressure on the physicochemical structure of char	[26]
Bituminous coal	Pressurized fixed bed	0.1–1.5 MPa	Yield distribution of pyrolysis products	[27]
Low-rank coal	Fluidized bed	0.1–0.7 MPa	Nitrogen and sulfur conversion	[28]
Coal	Fluidized bed	0.1–1.0 MPa	Distribution of pyrolysis products	[29]

Table 2
Proximate and ultimate analyses of Naomao Hu coal.

Proximate analysis (wt%, ad)				Ultimate analysis (wt%, ad)				
M	A	V	FC	C	H	O	N	S
2.65	5.31	46.26	45.78	60.68	3.27	26.98	0.74	0.37

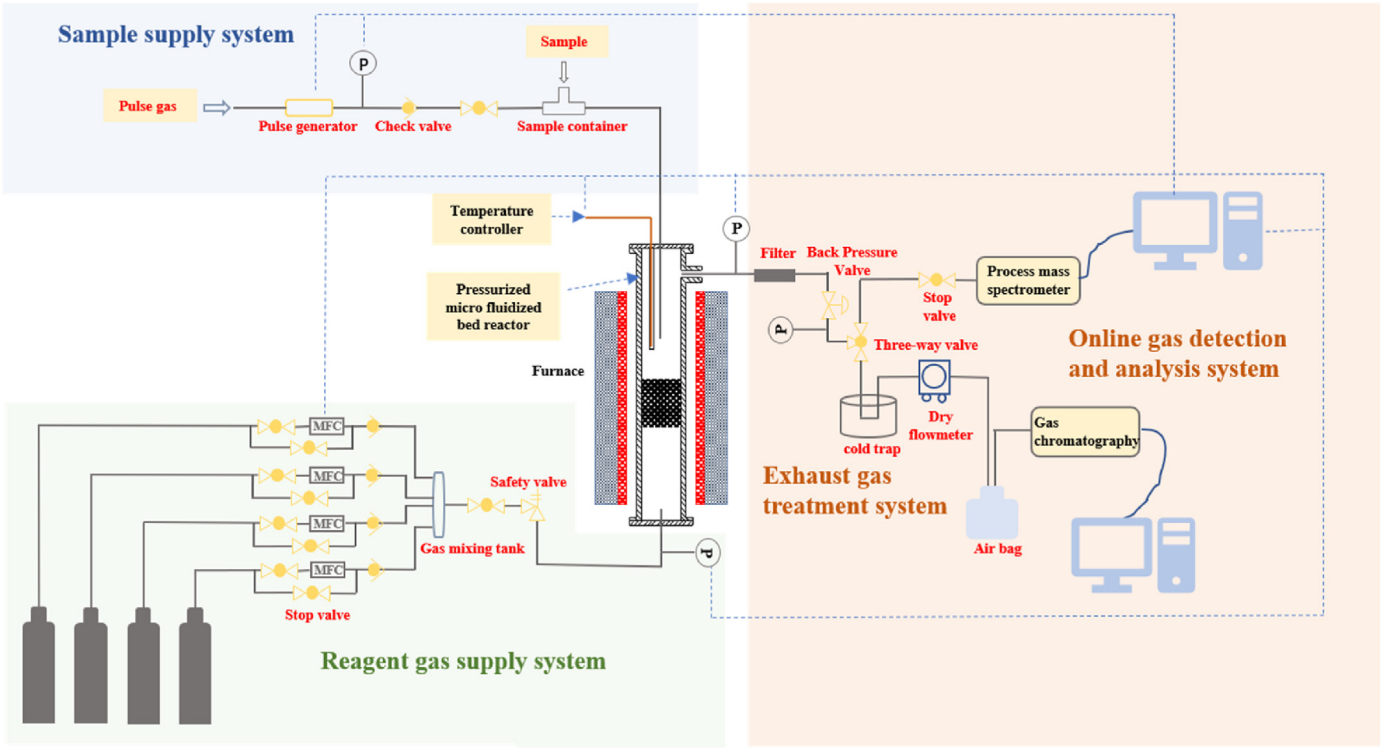

Fig. 1. Schematic diagram of the P-MFBRA system.

characteristics are analyzed, and the kinetic parameters are calculated.

2.3. Experimental operating parameters

Combining cold and hot state experiments and referring to the previous study [32] , the critical fluidization velocity of particles is determined by Eq. (1) :

$$u_{mf} = \frac{\mu\left[\sqrt{31.56^2 + 0.043Ar} - 31.56\right]}{d_p \rho_g} \quad (1)$$

The u_{mf} that makes the fluidized bed in a bubbling state is 1.5 cm s^{-1}, and the gas velocity of experiment is 3-5u_{mf}. The properties of gas change with the change of temperature and pressure. In order to keep the gas velocity constant, the flow rate must be changed accordingly. Firstly, the gas flow rate under different temperature and pressure was calculated according to the gas state equation. Then, a large number of pre-experiments were carried out for each working condition to verify the correctness of the calculated values, and then the gas flow rate was corrected with the mass spectrum curve. Comparative experiments are carried out on the selection of sample mass. Although the reaction is closer to the intrinsic reaction when the feed mass is small, the concentration of the gas product is too low to detect easily at this time, thereby the final sample mass at atmosphere is 8 mg. As the flow rate increases, the ratio of the feed mass to the flow rate must be controlled to a constant value, so that the gas products will not be diluted because of the increase of fluidized gas, thereby affecting the detection effect of MS. There are corresponding values of pulse pressure at different pressures. The specific parameters are shown in Table 3. To verify that the sample is fully in the reactor, click the solenoid valve switch twice for each sample injection. If there is almost no peak in MS for the second time, meaning that all the samples have entered the reactor for the first time. Each experiment is repeated several times with a relative error of less than 10%. The average value of three valid experimental data is used for kinetic analysis to ensure the reliability of experimental results.

2.4. Analysis methods

The release characteristics of each gas are monitored online by MS during pressurized isothermal pyrolysis process. Taking Fig. 2 as an example, the conversion rate is calculated as follows:

$$w_f = \frac{F \times \overline{C} \times M \times \left(t_f - t_0\right)}{22.4} \quad (2)$$

Table 3
Operating parameters for different conditions.

Number	Pressure MPa	Pulse pressure MPa	Temperature °C	Mass mg	Gas flow (mL·min^{-1})	Velocity (cm·s^{-1})
1	0.1	0.20	650	8.00	155	4.5
2	0.1	0.20	700	8.00	145	4.5
3	0.1	0.20	750	8.00	140	4.5
4	0.1	0.20	800	8.00	132	4.5
5	0.3	0.50	650	32.0	615	4.5
6	0.3	0.50	700	30.5	585	4.5
7	0.3	0.50	750	29.0	555	4.5
8	0.3	0.50	800	27.7	530	4.5
9	0.5	0.75	650	48.0	925	4.5
10	0.5	0.75	700	45.8	875	4.5
11	0.5	0.75	750	43.6	835	4.5
12	0.5	0.75	800	41.5	795	4.5
13	0.8	1.05	650	72.5	1385	4.5
14	0.8	1.05	700	68.8	1315	4.5
15	0.8	1.05	750	65.0	1250	4.5
16	0.8	1.05	800	62.3	1190	4.5
17	1.0	1.26	650	88.6	1695	4.5
18	1.0	1.26	700	84.1	1605	4.5
19	1.0	1.26	750	80.0	1530	4.5
20	1.0	1.26	800	76.3	1450	4.5

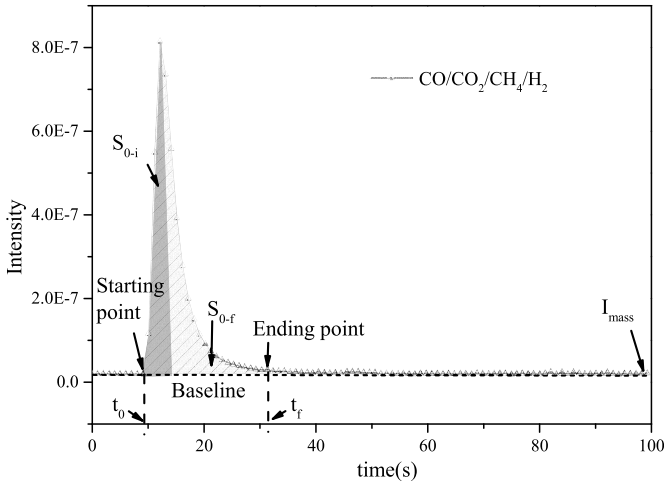

Fig. 2. Isothermal analysis method of coal pyrolysis.

$$w_i = w_f \times \frac{S_{0\to t_i}}{S_{0\to t_f}} = w_f \times \frac{\int_0^{t_i}(I_{mass}^{t_i} - I_{mass}^{t_0})dt}{\int_0^{t_f}\left(I_{mass}^{t_f} - I_{mass}^{t_0}\right)dt} \times 100\% \quad (3)$$

$$x_i = \frac{w_i}{w_f} = \frac{\int_0^{t_i}(I_{mass}^{t_i} - I_{mass}^{t_0})dt}{\int_0^{t_f}\left(I_{mass}^{t_f} - I_{mass}^{t_0}\right)dt} \times 100\% \quad (4)$$

$$R = -\frac{1}{w_f}\frac{d_{w_i}}{dt} = \frac{d_{x_i}}{dt} \quad (5)$$

where, w_i and w_f respectively represent the production for gases from the reaction starting time t_0 to arbitrary time t_i and the reaction ending time t_f. $S_{0\to t_i}$ and $S_{0\to t_f}$ represent the integrated areas between the baselines of each gases and the corresponding release curves measured by MS from t_0 to t_i and t_f, respectively. The meaning of I is the signal intensity of each gas tested by MS. F, $\overline{C}$, and M are the gas flow rate at standard state, the average concentration for gas, and the molar mass of each gas, respectively.

Typical reaction model functions are listed in Table 4 [33]. These functions have been extensively discussed in studies of the gas-solid reaction kinetics and proved to be suitable for describing the pyrolysis process of fuels.

3. Results and discussion

3.1. The influence of temperature and pressure on the yields of gases

The changes in total gas yield and the yields of four main gases at different temperatures and pressures are shown in Fig. 3. Due to the existence of secondary pyrolysis [23], with the increase of pyrolysis temperature and pressure, the degree of pyrolysis deepens and the yields of gas products increase. Comparing the influence of temperature and pressure on gas yield, the former has a greater influence. Temperature mainly affects the process of primary and secondary reactions of coal pyrolysis, while pressure mainly affects the secondary reactions process. The effect of pressure is significant and only becomes apparent when the pyrolysis temperature is above a certain critical temperature [18].

As temperature rises, the yields of four main gases improve, especially from 750 °C to 800 °C. Because the impacts of external and internal diffusion are obviously suppressed in P-MFBRA, the reaction rate greatly enhances, so that the reaction can proceed sufficiently. It can be seen from Fig. 3 that the variation of CO_2 yield with temperature is less than that of other gas components, and higher temperature is conducive to the generation of CO, CH_4 and H_2. The CO_2 produced by the primary reaction can be generated at low temperatures, thereby the generation of CO_2 less affected by the pyrolysis temperature. The significant increase in CO and H_2 yield is attributed to the effects of the primary and secondary reactions, and the secondary reaction is more violent under the higher temperature. With the elevation of temperature, both the generation of CH_4 and the probability of CH_4 cracking into H_2 increase. The competition between the two causes CH_4 yield not to increase continuously with temperature. The yield of H_2 increases significantly with the increasing temperature, which is related to the deepening of pyrolysis degree and the cracking of CH_4.

With the increase of pressure, the yields of CO_2 and CH_4 elevate observably. The CH_4 yield gains from 0.06 mL mg^{-1} under

Table 4
Common model functions in gas-solid reaction kinetics.

Model	Mechanism	G(x)	Symbol
G1	1-dimensional diffusion	x^2	
G2	2-dimensional diffusion	x+(1-x)ln (1-x)	
G3	3-dimensional diffusion (Jander)	$[1-(1-x)^{1/3}]^2$	
G4	3-dimensional diffusion (G-B)	$1-2x/3-(1-x)^{2/3}$	
G5	3-dimensional diffusion (A-J)	$[(1+x)^{1/3}-1]^2$	
G6	nucleation and growth n = 2/3	$[-\ln(1-x)]^{2/3}$	
G7	nucleation and growth n = 1/2	$[-\ln(1-x)]^{1/2}$	
G8	nucleation and growth n = 1/3	$[-\ln(1-x)]^{1/3}$	
G9	nucleation and growth n = 1/4	$[-\ln(1-x)]^{1/4}$	
G10	autocatalytic reaction	ln [x (1-x)]	
G11	Mampel power law n = 1/2	$x^{1/2}$	
G12	Mampel power law n = 1/3	$x^{1/3}$	
G13	Mampel power law n = 1/4	$x^{1/4}$	
G14	Reaction-order model, 3-order	$[(1-x)^{-2}-1]/2$	
G15	Reaction-order model, 2-order	$(1-x)^{-1}-1$	
G16	Reaction-order model, 1-order	-ln (1-x)	
G17	Reaction-order model, 0-order	x	
G18	phase interfacial reaction contraction sphere	$1-(1-x)^{1/3}$	
G19	phase interfacial reaction contraction cylinder	$1-(1-x)^{1/2}$	

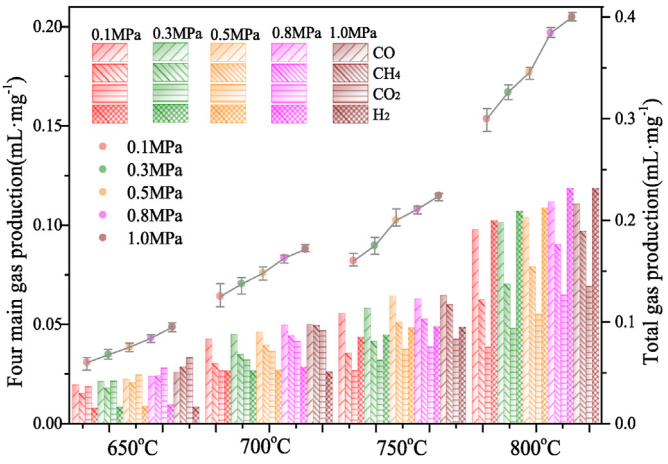

Fig. 3. Total gas yield and the yields of four main gases under different temperatures and pressures.

atmosphere to 0.097 mL mg^{-1} under pressurized condition at 800 °C. CH_4 is generated by H_2 infiltrating into and reacting with the newly formed active semi-coke after the volatiles escape during the pyrolysis process [34]. The higher pressure is beneficial to the diffusion of H_2 into the semi-coke pores, thereby favoring the generation of CH_4. Due to the different coal types and experimental conditions, the conclusions on the influence of pressure on H_2 and CO_2 production are not consistent. It is observed that there is no obvious law in the change of CO production with pressure, so the increase of CO_2 production may be connected to the CO-related reaction under pressurized condition. The yields of CO and H_2 increase significantly in the temperature axis and that of CO_2 and CH_4 increase obviously in the pressure axis respectively. The final yields of the four gases in the pyrolysis process is affected by both temperature and pressure.

3.2. The impact of temperature on the characteristics of gas release

Based on atmosphere and 0.5 MPa, the effect of temperature on gas-releasing characteristics is shown in Fig. 4. It can be seen from Fig. 4 that the influence of temperature on gas-releasing characteristics is reflected in gas evolution rate, gas-releasing sequence, gas-ending sequence, the total reaction time of gas, and gas proportion.

Under atmospheric condition, the total reaction time of gas changes little significantly with temperature because of the rapid isothermal reaction. However, gas evolution rate has changed obviously, among which H_2 is significantly enhanced, CH_4 and CO are also enhanced, but CO_2 is basically unchanged. This is because high temperature promotes pyrolysis reaction, and the chemical bonds of some long-chain macromolecules are broken to form a large number of small gas molecules [35]. Because of the difference in the gas evolution rate and the existence of secondary reactions, the proportion of CO_2 has a distinct decrease, that of CH_4 also has a downward trend, but those of H_2 and CO have increased evidently. The release sequence of four gases is CO_2, CO, CH_4 and H_2 at 650 °C. With the increase of temperature, the release of CO, CH_4 and H_2 is gradually advanced. At 800 °C, the difference in the release order of four gases reduces obviously, which is attributed to the fact that the difficulty between the cleavage and conversion of different groups reduces with increasing temperature. As the temperature rises, the end sequence of each gas is different, followed by CO_2, CH_4, H_2 and CO. The enhancement of secondary reaction at high temperature leads to the obvious trailing for CO and H_2 at the end of the reaction. The different release characteristic of each gas means its different generation paths and reaction mechanisms [30,31]. In the process of coal pyrolysis, the generation of CO_2 is mainly attributed to the cleavage of carboxyl groups and aliphatic rings [36]. Their bond energy is relatively weak, and cracking occurs at low temperatures. Compared with other gas components, H_2 is basically formed by volatiles through complex reactions that require higher temperature [13], so the release sequence of H_2 is the latest and the release intensity of H_2 is not obvious at 650 °C. CO is usually generated by the fracture of aliphatic ether and oxygen-containing carbonyl group at low temperatures and by the secondary cracking of volatiles at high temperatures, so both primary and secondary reactions will affect the generation of CO [36]. CH_4 is mainly derived from functional groups containing methyl groups in coal. Hence the release sequence of CO and CH_4 is between CO_2 and H_2.

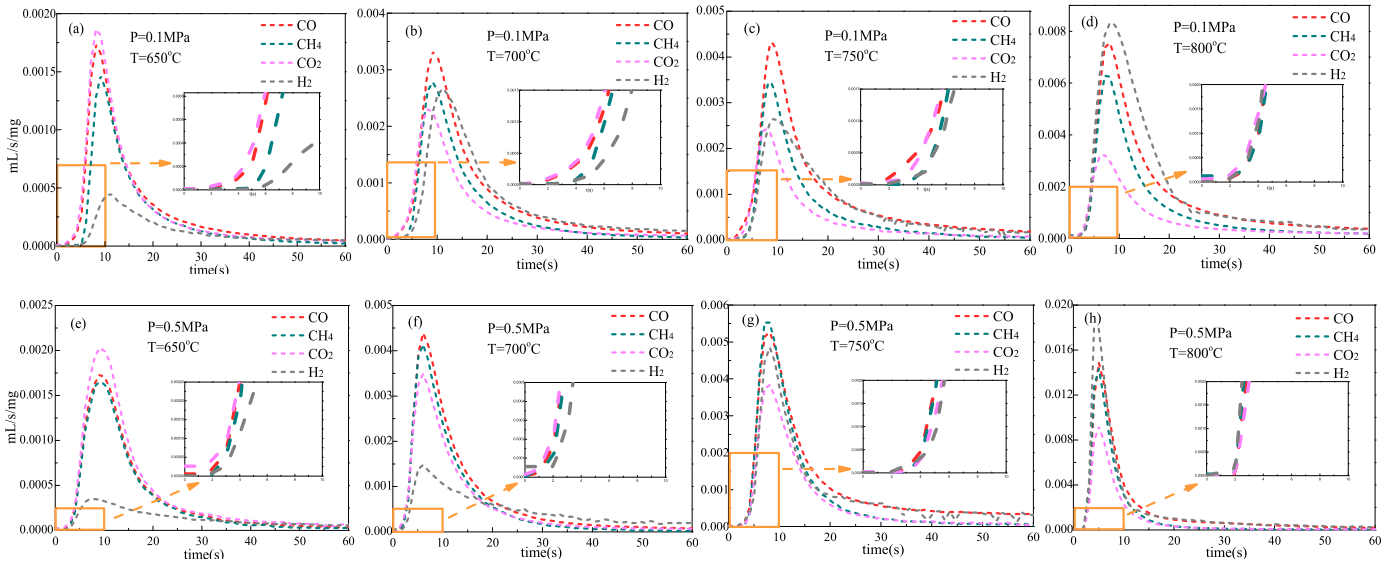

Fig. 4. The release characteristics of pyrolytic gases at different temperatures.

Under pressurized conditions, the difference of gas-releasing sequence reduces, indicating that the effect of pressure and temperature on gas-releasing sequence is synergistic. The basically same of gas-ending sequence indicates the pressure eliminates the influence of temperature on gas during the pyrolysis process. As the temperature increases, especially at 800 °C, the total gas reaction time is significantly shortened under 0.5 MPa, indicating that the effect of temperature and pressure on the gas evolution rate during coal pyrolysis is a synergistic effect, and both high temperature and high pressure will improve gas evolution rate.

3.3. *The impact of pressure on the characteristics of gas release*

At 650 and 800 °C, the release characteristics of four main gases during pyrolysis under different pressures are shown in Fig. 5. The influence of pressure on the pyrolysis process is limited by temperature [34]. At 650 °C, the pressure only affects the proportion of gas components. With the rise of pressure, the yields of four main gases increase. While the hydrogenation reaction and the endothermic reaction of carbon are more intense under pressure [37,38], so the ratio of CO_2 and CH_4 increases while that of CO and H_2 decreases. The reactions involved are shown in the following Eqs. (6)–(8). The final gas yield is competitively affected by the production and consumption of gas during the entire reaction process. Even if the proportion of gas decreases, the yield may increase.

$$CO\ (g) + H_2(g) — CH_4(g) + H_2O(g) \quad (6)$$

$$C\ (s) + H_2(g) — CH_4(g) \quad (7)$$

$$C\ (s) + CO_2(g) — 2CO\ (g) \quad (8)$$

The pressure affects the gas proportion, total reaction time and evolution rate at 800 °C. As pressure rises, the total gas reaction time first shortens and then extends, and the gas evolution rate first increases and then decreases. Both the reaction time is the shortest and the gas evolution rate is the largest at 0.5 MPa. The effect of pressure is embodied in two aspects. On the one hand, pressure will inhibit the escape of volatiles and reduce the mass transfer rate. On the other hand, the accumulation of light volatile gases will produce forced-flow, which will accelerate the escape of volatiles and

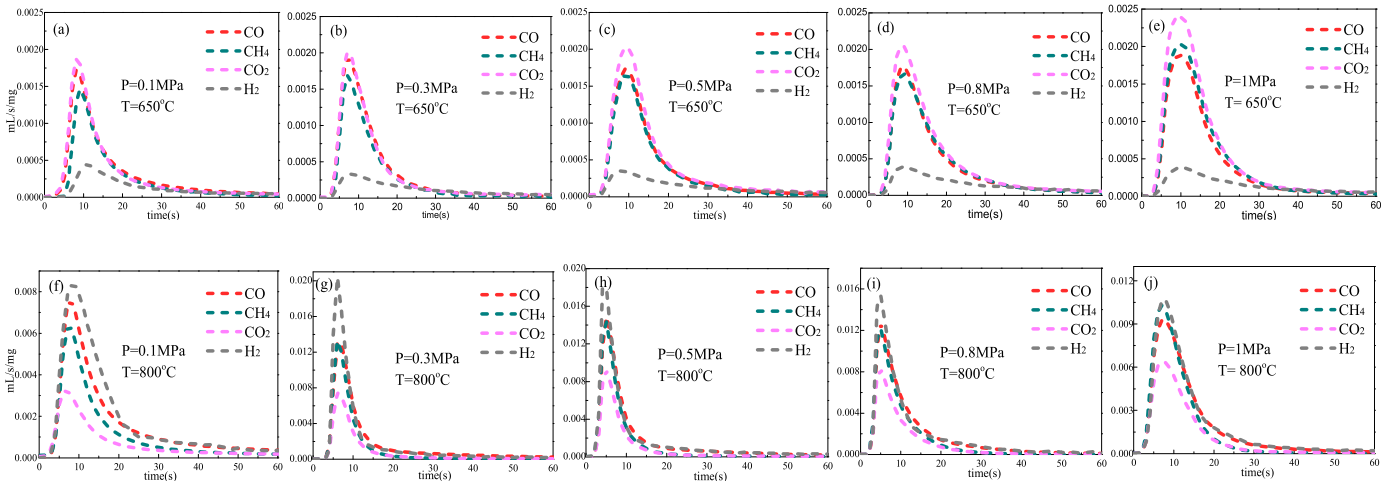

Fig. 5. The release characteristics of pyrolytic gases at different pressures.

increase the mass transfer rate [27]. Therefore, as pressure rises, forced-flow first dominates and then the inhibitory effect becomes more obvious. It can be seen from Fig. 5 that the difference in the sequence of gas-ending first reduces and then expands with pressure, indicating that the probability of secondary reactions increases, which confirms that the suppressive effect of pressure does dominate under high pressure. Whether at low or high temperature, the effect of pressure on gas-releasing sequence is not as obvious as that of temperature. There are differences in gas-releasing sequence at 650 °C and gas-ending sequence at 800 °C under atmosphere, respectively. But as the pressure rises, the difference gradually disappears. The change of gas proportion with pressure at 800 °C is the same as that at 650 °C, but it is more obvious at high temperature.

3.3.1. The influence of pressure and temperature on gas conversion rate

The conversion rate of 100% corresponds to the maximum gas yield at the end of pyrolysis. The reaction rate defined by the slope of the conversion curve elevates with increasing temperature, but the rate of increase in the reaction rate varies with gas components. The slope of the conversion curve of H_2 at atmosphere changes significantly with temperature, while that of the other three gases are not much different. When pressure rises from 0.1 MPa to 1.0 MPa, the conversion rate of each gas changes significantly first and then slowly with temperature. According to the above explanation, the influence of pressure is reflected in two aspects. Because the reaction process of generating H_2 is complicated, the pressure has a greater influence on it. The relationship between the conversion rate of the mixture gas and the time in pyrolysis process is shown in Fig. 6. It can be found that the conversion curve of a single gas component changes more obviously with temperature and pressure, indicating that there is a compensation or coupling effect between the reactions generating different gas components.

3.4. Calculation of kinetic parameters for coal pressurized isothermal pyrolysis

According to the release characteristics of different gas components, the isothermal pyrolysis kinetics of coal in P-MFBRA is analyzed:

$$\frac{dX}{dt} = k(T) \times f(x) \tag{9}$$

$$k(T) = Aexp\left(-\frac{E}{RT}\right) \tag{10}$$

where, $f(x)$ represents the differential mechanism function of the reaction, and $k(T)$ represents the Arrhenius rate constant, which is a constant in isothermal process. In this work, the integral method is used to calculate the kinetics of each gas generation process under different conditions [39]. The calculation equation is as follows:

$$G(x) = \int_0^x \frac{dx}{f(x)} = k(T) \times t \tag{11}$$

$$ln(k(T)) = \ln(A) - \frac{E}{RT} \tag{12}$$

where, $G(x)$ is the integral form of the mechanism function; E is the activation energy (Ea) , kJ·mol^{-1}; A is the pre-exponential factor, s^{-1} ; T is reaction temperature, K ; R is the gas constant , 8.314 J (mol^{-1} K^{-1}). Typical gas-solid reaction model functions are listed in Table 4. These functions have been widely used in studies of gas-solid reaction kinetics. A line is obtained by fitting $G(x)$-t based on Eq. (11) at a given temperature and pressure, and the slope of the line corresponds to $k(T)$. Finally, the influence of pressure on the kinetic parameters for coal pyrolysis is obtained.

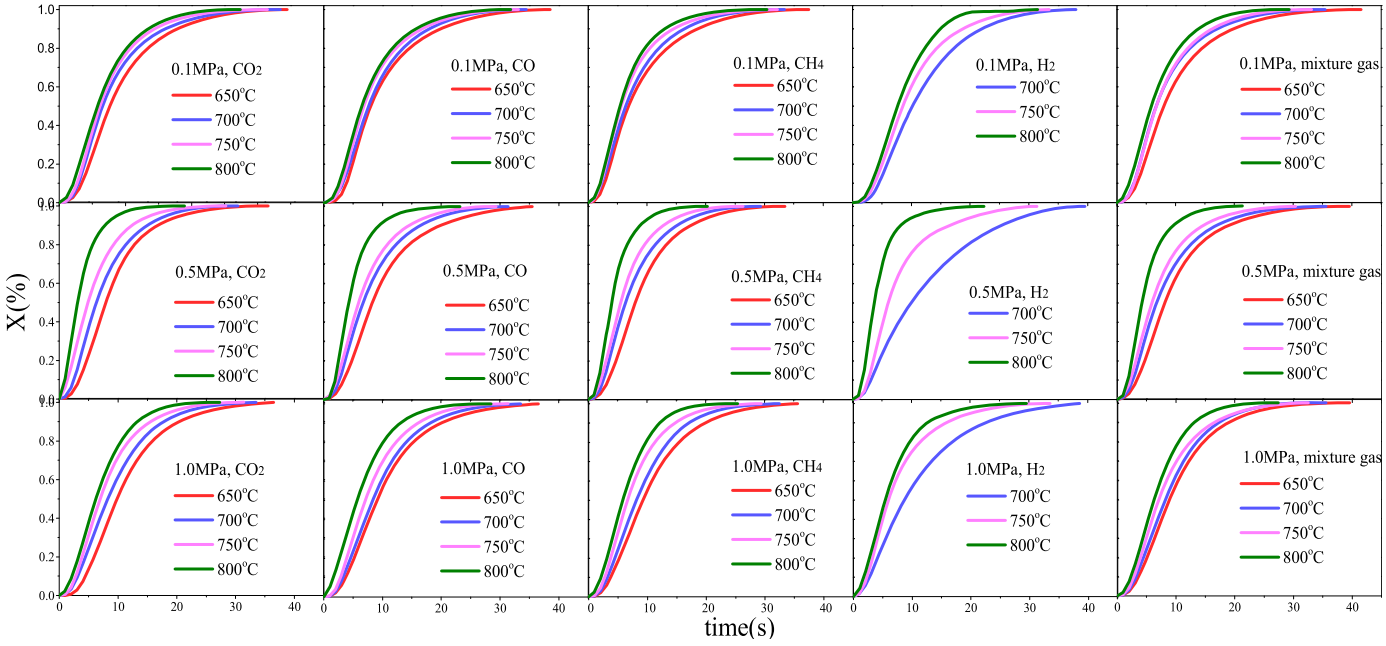

Fig. 6. Gas conversion rate versus reaction time at different temperatures for individual gas component and mixture gas.

Substituting 19 mechanism model functions into Eq. (11) for fitting the experimental data, it is found that the mechanism model functions with better degree of fitting for different gases are different under the same pressure. With the change of pressure, the mechanism model function with better degree of fitting for the same gas also changes. Three model functions which can better match the experimental data of each gas and model value are selected from 19 model functions after calculation. The results are shown in Fig. 7 and Table A1. The listed functions have a good linear relationship in the experimental data ranged the conversion of 0.1–0.9, indicating that coal pressurized pyrolysis does not just follow the first-order reaction model. The reaction mechanism varies with pressure, so the model that fits the experimental data well also changes. However, almost all pressurized non-isothermal reactions reported so far follow the first-order reaction model [20,22]. A diagram is drawn from the formulas to define the E and A for the four major gas components. The kinetic parameters obtained are shown in Table 5.

When different model functions fit the experimental data of one gas, there is little difference in the value of E yet a great difference in the values of *k(T)* and A, which is related to the reaction itself and different model functions. The relationship between *k(T)* calculated from model 18 and pressure is shown in Fig. 8. It can be found that the *k(T)* of the gas increases with temperature, while that first increases and then decreases with pressure and reaches the maximum value at 0.3 MPa, which is consistent with the analysis in Section 3.1.3. The reaction rate indicates how fast the reaction progresses. An elevation in pressure within a certain range increases the number of active sites on the surface of the char and accelerates the movement rate of volatiles, that is more obvious at high temperatures. However, the diffusion of volatiles is suppressed, and the carbon structure becomes more orderly beyond a certain pressure, which reduces the reaction rate. Hence, *k(T)* increases first and then decreases, and this trend is more obvious at high temperatures.

3.5. The most probable mechanism function model

The obtained kinetic parameters are substituted into *Eqs. (11) and (12)* to gain the calculated values of x based on different mechanism functions. Finally, the average relative error between the experimental values and calculated values is calculated through *Eq. (13)* to select the best probability mechanism function model. The function model with the smallest *OF* value is the most probable mechanism function [40], and the result is shown in Fig. 9 and Table 5.

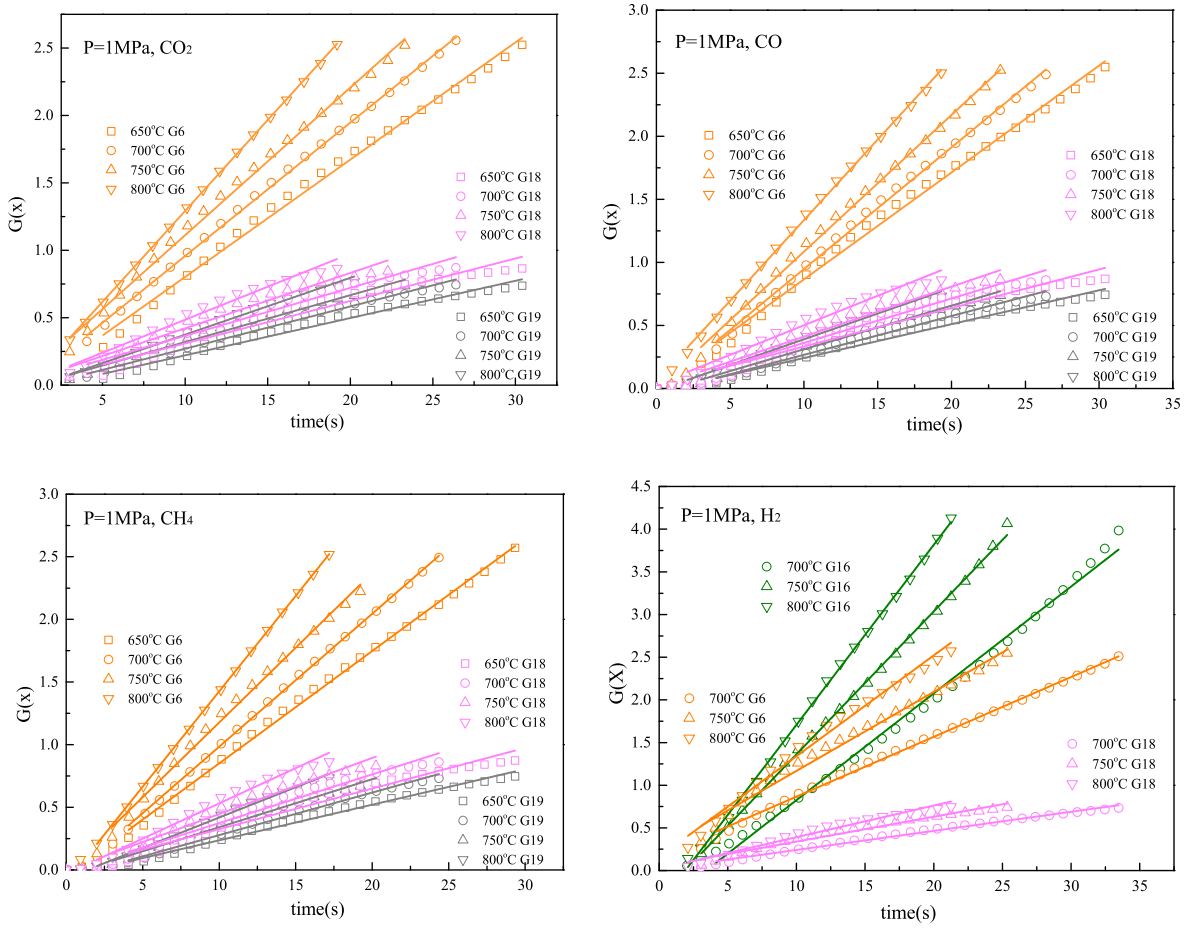

Fig. 7. The rate constants of coal at 1.0 MPa under different temperatures fitted by models.

Table 5
The pyrolysis kinetic parameters and OF value of each gas under different pressures.

Pressure/MPa	Gas	G(x)	E/kJ·mol^{-1}	A/s^{-1}	R^2	OF%
0.1	CO_2	6	14.85	0.63	0.97	4.49
		16	17.55	1.58	0.95	13.0
		18	13.21	0.16	0.95	3.40
	CO	6	15.32	0.59	0.99	5.52
		16	14.78	0.99	0.89	17.1
		18	13.37	0.15	0.97	6.21
	CH_4	6	19.37	1.11	0.95	8.37
		16	19.37	1.82	0.96	9.21
		18	20.05	0.36	0.96	4.17
	H_2	6	41.34	13.5	0.96	7.07
		7	43.19	12.2	0.95	9.71
		19	40.40	4.59	0.96	12.3
0.3	CO_2	2	27.00	1.48	0.93	20.3
		16	36.11	19.1	0.95	12.2
		18	30.41	1.59	0.95	6.31
	CO	2	36.19	4.38	0.97	18.3
		16	36.55	19.4	0.92	10.7
		18	33.02	2.08	0.95	5.38
	CH_4	2	48.74	21.9	0.92	18.3
		16	46.55	71.0	0.95	7.26
		18	42.79	7.33	0.95	5.66
	H_2	16	94.22	15707.3	0.96	13.1
		18	81.13	558.8	0.95	4.46
		19	88.23	1542.6	0.91	8.79
0.5	CO_2	3	39.61	3.55	0.93	18.9
		6	36.66	10.6	0.93	7.07
		18	37.61	3.75	0.92	4.54
	CO	6	39.12	12.8	0.92	5.61
		18	35.99	2.75	0.94	5.43
		19	34.95	2.74	0.94	10.3
	CH_4	6	37.46	11.9	0.92	3.79
		16	37.65	21.8	0.94	18.6
		18	36.10	3.17	0.96	6.92
	H_2	16	73.28	577.8	0.92	11.7
		18	69.11	112.9	0.92	6.18
		19	67.25	102.1	0.96	9.79
0.8	CO_2	16	29.70	6.95	0.95	16.2
		18	26.89	0.87	0.96	4.81
		19	26.72	0.94	0.96	8.00
	CO	6	27.17	2.72	0.99	4.88
		18	26.86	0.83	0.99	5.62
		19	25.98	0.84	0.99	9.05
	CH_4	6	28.95	3.74	0.95	4.35
		18	29.49	1.26	0.95	4.76
		19	31.33	1.81	0.97	8.44
	H_2	6	39.56	10.2	0.99	7.82
		16	43.24	27.9	0.99	12.7
		18	36.26	2.19	0.99	4.54
1.0	CO_2	6	23.59	1.83	0.95	3.57
		18	22.81	0.53	0.96	11.3
		19	24.49	0.75	0.98	8.39
	CO	6	22.55	1.58	0.98	3.77
		18	22.89	0.52	0.99	9.86
		19	23.42	0.64	0.99	9.06
	CH_4	6	28.42	3.56	0.96	4.48
		18	28.79	1.19	0.97	14.1
		19	29.93	1.57	0.98	9.42
	H_2	6	44.32	16.9	1	9.44
		16	44.33	30.5	0.99	10.4
		18	42.86	4.52	0.99	4.71

$$OF = \frac{1}{n}\sum_{n}\frac{\sqrt{(X_{exp} - X_{cal})^2}}{X_{exp}} \quad (13)$$

Fig. 9 compares the experimental and calculated data at representative temperature of 750 °C. With the change of pressure, the most probable mechanism function of each gas varies, and that of CO_2, CO and CH_4 change from G18 to G6 at 1 MPa, 0.8 MPa and 0.5 MPa, respectively, and H_2 changes from G6 to G18 at 0.3 MPa, indicating that the generation of gas involves different and complicated formation mechanisms.

G18-G19, the shrinking core model (SCM), believes that the reaction only occurs on the surface of the spherical reactant particles, and the reaction rate is affected by the unreacted surface area or the remaining amount of reactant. When the chemical reaction is a controlling step, the reaction order is 1/3 [41,42]. G6-G10 and G16, the homogeneous model (HM), assumes that the active sites inside the solid particles are uniformly distributed, and the particle size remains constant during the reaction, resulting in uniform changes in particle density. When the reaction order is 1, the chemical reaction is the controlling step [39]. The change of the most probable mechanism function shows that the reaction is completely controlled by chemistry at low pressure, but as pressure increases, the reaction conforms to G6 (HM model with reaction order not 1), indicating that it is affected by the diffusion effect. The average diffusion speed of gas is related to the relative mass of molecules [30], which makes the change of most probable mechanism function of each gas occur under different pressures. The generation mechanism of H_2 is complex and needs further research and discussion.

The Ea required to generate each gas calculated from the most probable mechanism function changes with pressure as shown in Fig. 10. The Ea represents the difficulty of generating each gas, which is related to the release sequence of each gas during pyrolysis process. Under atmospheric pressure, the order of Ea of each gas is $H_2CH_4COCO_2$. Because pressure changes the heat transfer inside the particles and leads to the competition between the secondary reaction of volatiles and the escape of volatiles [43], and the generation of light gases is affected by many factors. For the same gas, the Ea first increases and then decreases with pressure. The activation energies of H_2 and CH_4 reach the maximum at 0.3 MPa, and those of CO and CO_2 reach the maximum at 0.5 MPa, indicating that the thermal effect intensity and the ability for coal pyrolysis reaction are the maximum under this pressure condition. The difference in Ea of the four gases increases first and then decreases with pressure, indicating that the difficulty of generating each gas tends to be the same, which can be proved by the phenomenon that the gas-releasing tends to be consistent with the increase of pressure in Fig. 5. The difference in Ea between gases is mainly determined by H_2. H_2 is the most difficult to generate at 0.3 MPa, so the difference in Ea between gases increases between 0.1 and 0.3 MPa.

3.6. Comparison of kinetic parameters in P-TGA and P-MFBRA

The most probable mechanism function for mixture gas during pyrolysis process and isothermal pyrolysis kinetic parameters of the mixture gas are shown in Fig. 11. It is found that the most probable mechanism function of mixture gas changes from G16 to G6 before and after 0.5 MPa. It is known that the HM model with a reaction order of 1 indicates that the pyrolysis process is only controlled by chemistry. As pressure increases, the reaction order is less than 1, indicating that the reaction is affected by diffusion. Since the 19 models in Table 4 are all suitable for atmosphere, the value of R^2 obtained under pressurized conditions is low. Therefore, the model needs to be revised in the subsequent studies to derive a

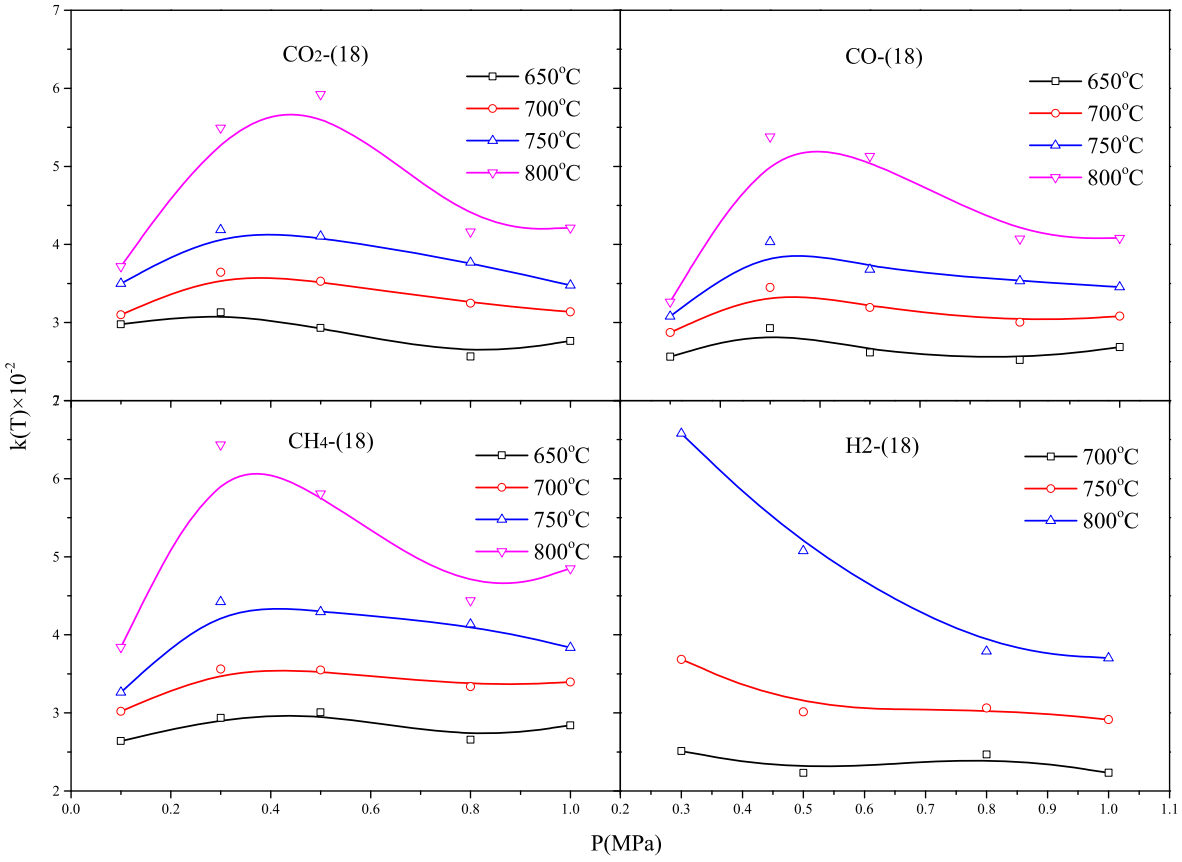

Fig. 8. The reaction rate for the four main gases calculated based on G18 model under different pressures.

kinetic model suitable for pressurized conditions. Fig. 11(b) depicts the Ea and rate constant of the mixture gas as a function of pressure. The Ea of mixture gas is greatly affected by that of H_2. The value of *k(T)* is related to the selection of the model. Although the most probable mechanism model of the mixture gas is different from that of the individual gas, the calculated *k(T)* still increases first and then decreases with pressure.

Table 6 is a comparison of non-isothermal and isothermal kinetic results. The effect of pressure on pyrolysis is closely related to residence time [45]. Compared the measurements in P-TGA, the values of E and A are obviously lower, indicating the quick pyrolysis reaction in the P-MFBRA. The value of E represents the difficulty for starting the reaction, and that of A means the effective collision of reactant molecules [13]. A lower value of E means that the reaction is easier to start and occur, so fewer reactant molecules are required to collide. This is consistent with the characteristics of P-MFBRA, which is to heat the particles at a high rate and minimize the diffusion inhibition of the reaction. As pressure rises, the value of E for P-TGA increases, but that for P-MFBRA first increases and then decreases. The isothermal pyrolysis experiment eliminated the effect of reaction time on pressure, resulting in a more significant effect of pressure on pressurized pyrolysis process for low-rank coal.

4. Conclusions

In this work, the effects of temperature and pressure on the characteristics of gas release and kinetics during coal pressurized isothermal pyrolysis process are explored in the P-MFBRA, and the kinetic parameters of pressurized non-isothermal and isothermal pyrolysis are compared. The conclusions are as follows:

1) The output of the four main gases (CO_2, CO, CH_4, H_2) increases with temperature and pressure, but the effect of temperature on gas yield is greater than that of pressure. Under atmosphere, the order of gas-releasing is CO_2, CO, CH_4, H_2 at 650 °C and that of gas-ending is CO_2, CH_4, H_2, and CO at 800 °C.
2) The difference in the order of gas-releasing reduces as temperature and pressure rises, but that of gas-ending first decreases and then increases with pressure. As temperature rises, the total gas-releasing time is basically unchanged at atmosphere and significantly shortened at 0.5 MPa. With the increasing pressure,

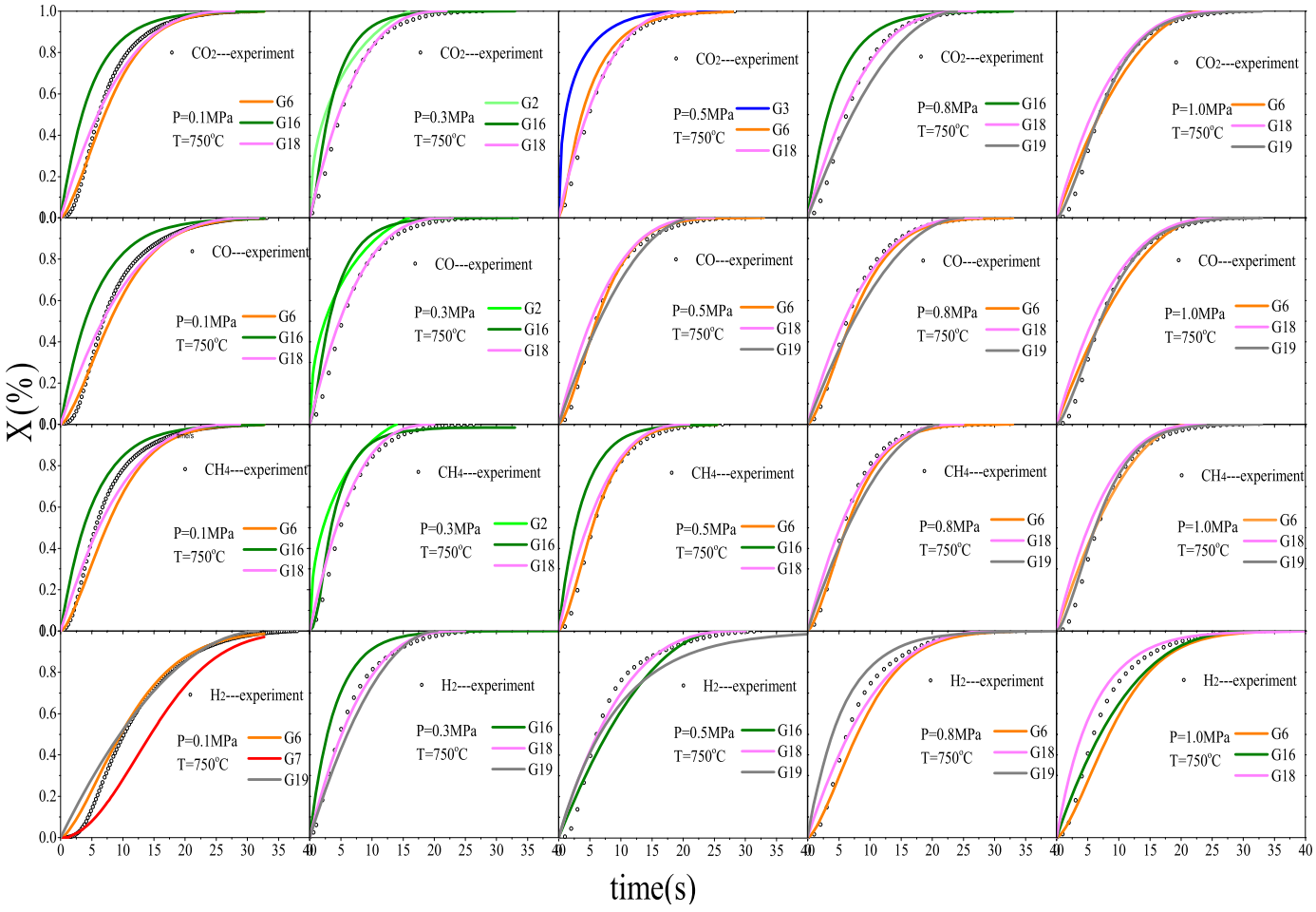

Fig. 9. Comparison of experimental data and calculated value obtained by different mechanism models for coal pressurized pyrolysis under different pressures at 750 °C.

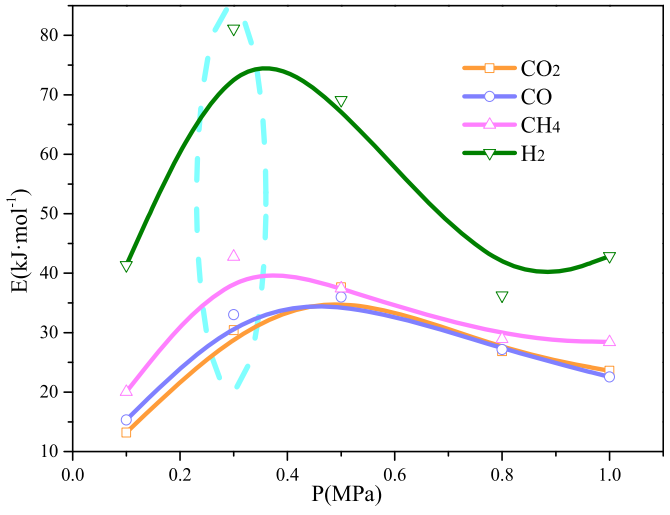

Fig. 10. The Ea of each gas calculated based on the most probable mechanism function under different pressures.

the gas-releasing rate does not change obviously at 650 °C, while that first increases and then decreases at 800 °C related with the competitive reaction of the release of volatiles and the secondary pyrolysis of volatiles caused by pressure.

3) The difference in the most probable mechanism model of each gas indicates that the reaction does not only follow the first-order reaction. With the change of pressure, the most probable mechanism function of each gas varies, and that of CO_2, CO and CH_4 change from G18 to G6 at 1 MPa, 0.8 MPa and 0.5 MPa, respectively. The change of the most probable mechanism function shows that reaction under low pressure is completely controlled by chemistry, but reaction is affected by the diffusion effect with elevating pressure.
4) With the increase of pressure, the rate constant and Ea of each gas appear an increasing-decreasing tendency, the difference between Ea of each gas reduces, and the degree of difficulty of gas generation approaches. Pressure has the greatest influence on H_2, and the change in the Ea of mixture gas is related to that of H_2.
5) Compared with the non-isothermal experiments, the Ea and pre-exponential factor in P-MFBRA are less than those in P-TGA, indicating P-MFBRA can effectively reduce the diffusion inhibition, and the kinetics obtained is close to the actual reaction in the industrial fluidized bed reactor. Existing dynamics models are based on atmospheric pressure, the fitting degree obtained under pressurized conditions is low. Therefore, the model needs to be revised in the subsequent studies to derive a kinetic model suitable for pressurized conditions.

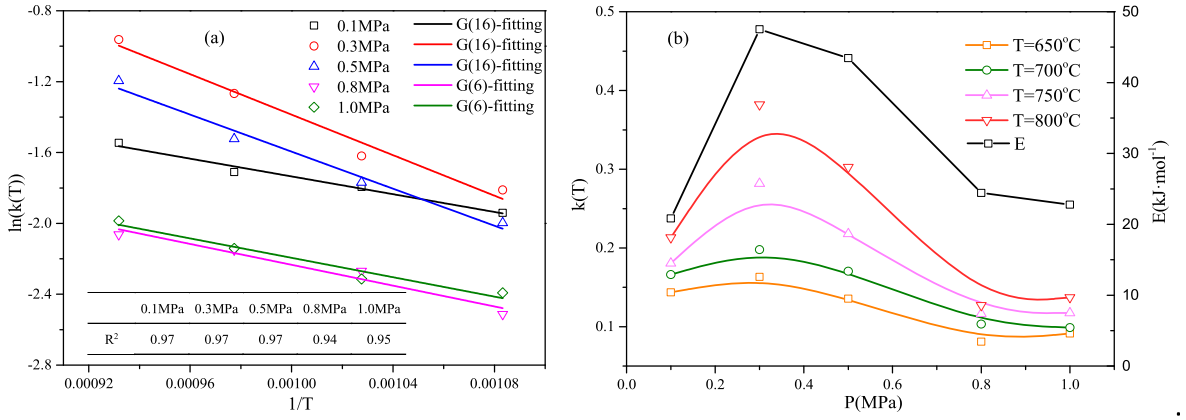

Fig. 11. (a) Arrhenius equation for activation energy based on the probable mechanism function for coal pressurized pyrolysis, (b) The rate constant and Ea for mixture gas calculated based on the most probable mechanism function under different pressures.

Table 6
Comparison of kinetic data for solid fuels pyrolysis in different reactions.

Sample	Pressure	E/(kJ·mol^{-1})	A/(s^{-1})	Reactor	Ref.
Bituminous coal	0.1	76.7	6.82×10^2	P-TGA (10 K·min^{-1})	[44]
	0.4	123	5.60×10^6		
	1.0	150	9.80×10^8		
Hanqiao coal	0.1	70.0	2.00×10^7	P-TGA (20 K·min^{-1})	[18]
	0.5	87.6	6.00×10^8		
	0.9	95.9	3.10×10^9		
	1.3	103	1.10×10^{10}		
Low-rank coal	0.1	20.8	2.16	P-MFBRA	This study
	0.3	47.5	75.9		
	0.5	43.5	37.8		
	0.8	24.4	2.02		
	1.0	22.8	1.72		

Declaration of competing interest

The authors declare that they have no known competing financial interests or personal relationships that could have appeared to influence the work reported in this paper.

Acknowledgments

This research was financially supported by the Fundamental Research Funds for the National Key R&D Program of China (2019YFE0100100-05). Thanks to the team of Professor Guangwen Xu from the Institute of Engineering Processes of the Chinese Academy of Sciences for the technical guidance on the use of the pressurized micro-fluidized bed reaction analyzer developed by them.

Credit author statement

Zhu Yao: Experimental methods, Experiment, Data processing, and Writing. **Wang Qinhui**: Experimental design, Communication. **Li Kaikun**: Experiment. **Cen Jianmeng**: Communication. **Fang Mengxiang**: Data analysis, Language modification. **Ying Chengdong**: Language modification.

Appendix A. Supplementary data

Supplementary data to this article can be found online at https://doi.org/10.1016/j.energy.2021.122475.

References

[1] Aydin G. Forecasting natural gas production using various regression models. Petrol Sci Technol 2015;33(15):1486–92.
[2] Du L, Zhao H, Tang H, Jiang P, Ma W. Analysis of the synergistic effects of air pollutant emission reduction and carbon emissions at coal-fired power plants in China. Environ Prog Sustain Energy 2021;40:1–10.
[3] Jie D, Xu X, Guo F. The future of coal supply in China based on non-fossil energy development and carbon price strategies. Energy 2021;220:119644.
[4] Guo L, Ding Y, Liao Q, Zhu X, Wang H. A new heat supply strategy for CO_2 capture process based on the heat recovery from turbine exhaust steam in a coal-fired power plant. Energy 2022;239:121817.
[5] Li C, Zhao J, Fang Y, Wang Y. Pressurized fast-pyrolysis characteristics of typical Chinese coals with different ranks. Energy Fuel 2009;23(10):5099–105.
[6] Hong J, Chaudhry G, Brisson JG, Field R, Gazzino M, Ghoniem AF. Analysis of oxy-fuel combustion power cycle utilizing a pressurized coal combustor. Energy 2009;34(9):1332–40.
[7] Gai C, Dong Y, Zhang T. The kinetic analysis of the pyrolysis of agricultural residue under non-isothermal conditions. Bioresour Technol 2013;127:298–305.
[8] Guo X, Cai J, Yu X. Kinetics and thermodynamics of microalgae residue oxidative pyrolysis based on double distributed activation energy model with simulated annealing method. J Anal Appl Pyrol 2021;154:104997.
[9] Du J, Gao L, Yang Y, Chen G, Guo S, Omran M, et al. Study on thermochemical characteristics properties and pyrolysis kinetics of the mixtures of waste corn stalk and pyrolusite. Bioresour Technol 2021;324:124660.
[10] Wang F, Zeng X, Geng S, Yue J, Tang S, Cui Y, et al. Distinctive hydrodynamics of a micro fluidized bed and its application to gas–solid reaction analysis. Energy Fuel 2018;32:4096–106.
[11] Li J, Dou B, Zhang H, Zhang H, Chen H, Xu Y, et al. Pyrolysis characteristics and non-isothermal kinetics of waste wood biomass. Energy 2021;226:120358.
[12] Zeng X, Zhang J, Adamu MH, Wang F, Han Z, Zheng Q, et al. Behavior and kinetics of drying, pyrolysis, gasification, and combustion tested by a micro-fluidized bed reaction analyzer for the staged-gasification process. Energy Fuel 2020;34(2):2553–65.
[13] Yu J, Yao C, Zeng X, Shuang G, Li D, Yin W, et al. Biomass pyrolysis in a micro-fluidized bed reactor: characterization and kinetics. Chem Eng J 2011;168(2):839–47.

[14] Jian Y, Yue J, Liu Z, Li D, Xu G, Zhu J, et al. Kinetics and mechanism of solid reactions in a micro fluidized bed reactor. Aiche J 2010;56(11):2905–12.
[15] Zabaniotou A, Damartzis T. Modelling the intra-particle transport phenomena and chemical reactions of olive kernel fast pyrolysis. J Anal Appl Pyrol 2007;80(1):187–94.
[16] Manyà J, Arauzo J. An alternative kinetic approach to describe the isothermal pyrolysis of micro-particles of sugar cane bagasse. Chem Eng J 2008;139(3):549–61.
[17] Wang F, Zeng X, Wang Y, Su H, Yu J, Xu G. Non-isothermal coal char gasification with CO_2 in a micro fluidized bed reaction analyzer and a thermogravimetric analyzer. Fuel 2016;164(15):403–9.
[18] Sun CL, Xiong YQ, Liu QX, Zhang MY. Thermogravimetric study of the pyrolysis of two Chinese coals under pressure. Fuel 1997;76(7):639–44.
[19] Yang H, Chen H, Ju F, Yan R, Zhang S. Influence of pressure on coal pyrolysis and char gasification. Energy Fuel 2007;21(6):3165–70.
[20] Yan L, He B, Hao T, Pei X, Li X, Wang C, et al. Thermogravimetric study on the pressurized hydropyrolysis kinetics of a lignite coal. Int J Hydrogen Energy 2014;39(15):7826–33.
[21] Wang G, Hou B, Zhang J, Wang H, Gao D, Chang G, et al. Effect of pressure and H_2 on the pyrolysis characteristics of lignite: thermal behavior and coal char structural properties. J Anal Appl Pyrol 2018;135:1–9.
[22] Yan L, He B, Hao T, Pei X, Li X. Pressurized thermogravimetric study on the hydropyrolysis and hydrogasification kinetics of a bituminous coal. Energy Fuel 2012;28(5):2993–3001.
[23] Zhou G, Zhong W, Yu A, Dou Y, Yin J. Experimental study on characteristics of pressurized grade conversion of coal. Fuel 2018;234:965–73.
[24] Gao S, Zhai L, Qin Y, Wang Z, Zhao J, Fang Y. Investigation into the cleavage of chemical bonds induced by CO_2 and its mechanism during the pressurized pyrolysis of coal. Energy Fuel 2018;32(3):3243–53.
[25] Tahmasebi A, Maliutina K, Yu J. Impact of pressure on the carbon structure of char during pyrolysis of bituminous coal in pressurized entrained-flow reactor. Kor J Chem Eng 2019;36(3):393–403.
[26] Zhang W, Zhao Y, Sun S, Feng D, Li P. Effects of pressure on the characteristics of bituminous coal pyrolysis char formed in a pressurized drop tube furnace. Energy Fuel 2019;33(12):12219–26.
[27] Luo K, Zhang C, Zhu S, Bai Y, Li F. Tar formation during coal pyrolysis under N_2 and CO_2 atmospheres at elevated pressures. J Anal Appl Pyrol 2016;118:130–5.
[28] Duan Y, Duan L, Anthony EJ, Zhao C. Nitrogen and sulfur conversion during pressurized pyrolysis under CO_2 atmosphere in fluidized bed. Fuel 2017;189:98–106.
[29] Chen Z, Gao S, Xu G. Simultaneous production of CH_4-rich syngas and high-quality tar from lignite by the coupling of noncatalytic/catalytic pyrolysis and gasification in a pressurized integrated fluidized bed. Appl Energy 2017;208:1527–37.
[30] Mao Y, Dong L, Dong Y, Liu W, Chang J, Yang S, et al. Fast co-pyrolysis of biomass and lignite in a micro fluidized bed reactor analyzer. Bioresour Technol 2015;181:155–62.
[31] Zhang Y, Zhao M, Linghu R, Wang C, Zhang S. Comparative kinetics of coal and oil shale pyrolysis in a micro fluidized bed reaction analyzer. Carbon Resour Conv 2019;2(3):217–24.
[32] Lin L, Duan Y, Duan L, Xu C, John AE. Flow characteristics in pressurized oxy-fuel fluidized bed under hot condition. Int J Multiphas Flow 2018;108:1–10.
[33] Feng D, Guo D, Zhao Y, Zhang Y, Geng K, Chang G, et al. In-situ decoupling effect of H_2O on the whole process of coal gasification in MFBRA and TG-FTIR-MS. J Anal Appl Pyrol 2020;145. 104744.1-.11.
[34] Reichel D, Siegl S, Neubert C, Krzack S. Determination of pyrolysis behavior of brown coal in a pressurized drop tube reactor. Fuel 2015;158:983–98.
[35] Zhong M, Zhang Z, Zhou Q, Yue J, Gao S, Xu G. Continuous high-temperature fluidized bed pyrolysis of coal in complex atmospheres: product distribution and pyrolysis gas. J Anal Appl Pyrol 2012;97:123–9.
[36] Banyasz JL, Li S, Lyons-Hart JH, Shafer KH. Gas evolution and the mechanism of cellulose pyrolysis. Fuel 2001;80(12):1757–63.
[37] Yan S, Bi J, Qu X. The behavior of catalysts in hydrogasification of sub-bituminous coal in pressured fluidized bed. Appl Energy 2017;206:401–12.
[38] Wang Y, Bell DA. Reaction kinetics of powder river basin coal gasification in carbon dioxide using a modified drop tube reactor. Fuel 2015;140:616–25.
[39] Zhang Y, Yao M, Gao S, Sun G, Xu G. Reactivity and kinetics for steam gasification of petroleum coke blended with black liquor in a micro fluidized bed. Appl Energy 2015;160:820–8.
[40] Capart R, Khezami L, Burnham AK. Assessment of various kinetic models for the pyrolysis of a microgranular cellulose. Thermochim Acta 2004;417(1):79–89.
[41] Chen G, Omran M, Li K, Jiang Q, Chen J. Kinetics characteristics and microwave reduction behavior of walnut shell-pyrolusite blends. Bioresour Technol 2021;319(3):124172. https://doi.org/10.1016/j.biortech.2020.124172.
[42] Wang F, Zeng X, Wang Y, Yu J, Xu G. Characterization of coal char gasification with steam in a micro-fluidized bed reaction analyzer. Fuel Process Technol 2016;141:2–8.
[43] Griffin TP, Howard JB, Peters WA. Pressure and temperature effects in bituminous coal pyrolysis: experimental observations and a transient lumped-parameter model. Fuel 1994;73(4):591–601.
[44] Park DK, Song E. Pressurized pyrolysis characteristics of two ranks of coal in a thermogravimetric analyzer. J Energy Eng 2017;143(5):1–10.
[45] Howaniec N. The effects of pressure on coal chars porous structure development. Fuel 2016;172:118–23.